

1 Organic matters, but inorganic matters too: column examination  
2 of elevated mercury sorption on low organic matter aquifer  
3 material using concentrations and stable isotope ratios.

4 David S. McLagan<sup>1,2,3,\*</sup>, Carina Esser<sup>1,\*</sup>, Lorenz Schwab<sup>4,5</sup>, Jan G. Wiederhold<sup>4</sup>, Jan-  
5 Helge Richard<sup>6</sup>, Harald Biester<sup>1</sup>.

6 1 - Institute of Geoecology, Technische Universität Braunschweig, Braunschweig, 38106, Germany.

7 2 - Department of Geological Sciences and Geological Engineering, Queen's University, Kingston, ON, K7L3N6, Canada.

8 3 - School of Environmental Studies, Queen's University, Kingston, ON, K7L3J6, Canada.

9 4 - Department for Environmental Geosciences, Centre for Microbiology and Environmental Systems Science, University  
10 of Vienna, Vienna, 1090, Austria.

11 5 - Environmental Engineering Institute IIE-ENAC, Soil Biogeochemistry Laboratory, Ecole Polytechnique Fédérale de  
12 Lausanne (EPFL), Sion, Switzerland.

13 6 - Institute for Hygiene and Environment Hamburg, 20539 Hamburg, Germany

14 \* - These authors contributed equally to the manuscript.

15 Correspondence to: david.mclagan@queensu.ca

16

## 17 Abstract

18 Sorption of mercury (Hg) in soils is suggested to be predominantly associated with organic matter  
19 (OM). However, there is a growing collection of research that suggests clay minerals and Fe/Mn-  
20 oxides are also important solid-phases for the sorption of soluble Hg in soil-groundwater systems.  
21 We use a series of (60 mL syringe based) column experiments to examine sorption and subsequent  
22 desorption of HgCl<sub>2</sub> solutions (Experiment 1 [EXP1]: 46.1 ± 1.1 mg L<sup>-1</sup>; and Experiment 2 [EXP2]: 144  
23 ± 6 mg L<sup>-1</sup>) in low OM (0.16 ± 0.02 %) solid-phase aquifer materials. Analyses of total Hg  
24 concentrations, Hg speciation (i.e., pyrolytic thermal desorption (PTD)), and Hg stable isotopes are  
25 performed on both solid- and liquid-phase samples across sorption and desorption phases.

26 Sorption breakthrough curve best fitted a Freundlich model. Despite the very low OM content, the  
27 Hg equilibrium sorptive capacity in these columns is very high: 1510 ± 100 and 2320 ± 60 mg kg<sup>-1</sup> for  
28 the EXP1 and EXP2, respectively, and is similar to those determined for high OM soils. Data from the  
29 experiments on mass dependent fractionation of Hg stable isotope fractionation data (described by  
30 δ<sup>202</sup>Hg) support preferential sorption of lighter isotopes to the solid-phase materials with results  
31 indicating isotopically heavier liquid-phase and isotopically lighter solid-phase. Desorption fits  
32 exponential decay models and 46 ± 6% and 58 ± 10% of the sorbed Hg is removed from the solid-  
33 phase materials at the termination of desorption in EXP1 and EXP2, respectively. The divergence of  
34 δ<sup>202</sup>Hg values between liquid- and solid-phase also continues into desorption. This desorption  
35 profile is linked to the initial release of easily exchangeable Hg(II) species physically sorbed to  
36 Fe/Mn-oxides and clay mineral surfaces (liquid-phase enriched in heavy isotopes) and then slower  
37 release of Hg(II) species that have undergone secondary reaction to more stable/less soluble Hg(II)  
38 species and/or diffusion/transport into the mineral matrices (processing favouring lighter isotopes;  
39 solid-phase enriched in lighter isotopes). The secondary production of Hg(0) within the columns is  
40 confirmed by PTD analyses that indicate distinct Hg(0) release peaks in solid-phase samples at <175  
41 °C, which again agree with field observations. Retardation (R<sub>D</sub>) and distribution (K<sub>D</sub>) coefficients are  
42 77.9 ± 5.5 and 26.1 ± 3.0 mL g<sup>-1</sup> in EXP1, respectively, and 38.4 ± 2.7 and 12.4 ± 0.6 mL g<sup>-1</sup> in EXP2,  
43 respectively. These values are similar to values derived from column experiments on high OM soil  
44 and provide the basis for future Hg fate and transport modelling in soil-groundwater systems.

45 **Keywords:** Mercury stable isotopes, column experiments, sorption/desorption, groundwater,  
46 polluted sites, distribution coefficient.

## 47 1 Introduction

48 Mercury (Hg), a transition metal of group 12 and period 6 of the periodic table, has a unique  
49 electrochemical structure. The pair of electrons in the outermost (6s) shell have a relativistically  
50 contracted radius, which greatly reduces the element's ability to form metal-metal bonds (Norrby,  
51 1991). Hence, Hg is the only liquid-phase metal at standard temperature and pressure. Even with  
52 this radial contraction, Hg is an atomically large element, and species in its divalent oxidation state  
53 qualify as "soft-acids", which under hard and soft Lewis acid and base theory results in Hg having  
54 greater affinity for "soft-bases" (Ho, 1975). One particularly pertinent "soft-base" for Hg is sulphur.  
55 Cinnabar (α-HgS) and meta-cinnabar (β-HgS) are the dominant forms of Hg in the lithosphere  
56 (Gettens et al., 1972; Clarkson, 1997), but are relatively stable ores that have very low solubility,  
57 and bioavailability (Llanos et al., 2011; Lu et al., 2011). Mining of these cinnabar ores for industrial  
58 use of Hg has heavily perturbed the natural biogeochemical cycle of Hg. Other primary sources of  
59 Hg emissions/releases to the environment include geogenic (natural), fossil-fuel combustion,

60 industrial and medical uses of Hg, and legacy emissions from Hg polluted sites (Pirrone et al., 2010;  
61 Kocman et al., 2013; Streets et al., 2019).

62 While redox conditions and organic matter (OM) availability and composition are key determinants  
63 in the mobility of Hg in aquatic/saturated subsurface environments, pH (Andersson, 1979; Gu et al.,  
64 2011; Manceau and Nagy, 2019), chloride concentration ( $\text{Cl}^-$ ; Schuster, 1991), and speciation of Hg  
65 inputs (particularly for polluted systems; McLagan et al., 2022) also play important roles. Solubilities  
66 of Hg species vary widely from practically insoluble cinnabar species ( $\approx 2 \cdot 10^{-24} \text{ g L}^{-1}$ ) to low solubility  
67 elemental Hg ( $\text{Hg}(0)$ :  $\approx 5 \cdot 10^{-5} \text{ g L}^{-1}$ ) to highly soluble Hg(II)-chloride ( $\text{HgCl}_2$ ) ( $66 \text{ g L}^{-1}$ ) (Sanemasa,  
68 1975; Schroeder and Munthe, 1998; Skyllberg et al., 2012). In systems that are OM limited, clay  
69 minerals and oxides, hydroxides, and oxyhydroxides of Fe, Mn and Al become increasingly important  
70 sorbents for Hg species (Lockwood and Chen, 1973; Schuster 1991; Kim et al., 2004). Additionally,  
71 there is a strong tendency of Hg(II) to complex with hydroxides and halides under oxic conditions  
72 (Schuster, 1991, Ullrich et al., 2001). Uptake of Hg to inorganic sorbents has been reported to occur  
73 via rapid initial surface sorption followed by slower phase of Hg undergoing secondary  
74 transformation to more stable/less soluble species or diffusing into the mineral matrices (Avotins,  
75 1975; Miretzky et al., 2005; McLagan et al., 2022).

76 More recently, laboratory and field studies have expanded biogeochemical assays of Hg in  
77 subsurface environments using stable isotopes (Jiskra et al., 2012; Zheng et al., 2018; McLagan et  
78 al., 2022). Hg is an isotopic system that has seven stable isotopes and to which environmental  
79 processes can impart mass-dependent (MDF) as well as both odd and even mass-independent (MIF)  
80 fractionation (Bergquist and Blum, 2007; 2009; Wiederhold, 2015). In particular, this capacity for Hg  
81 stable isotope analyses to elicit valuable information on tracing/identifying specific environmental  
82 processes make them a vital tool in the examination of Hg biogeochemical cycling (Bergquist and  
83 Blum, 2007; 2009; Wiederhold, 2015).

84 Traditionally, column and batch experiments have been utilised to assess the sorption (including  
85 sorption or distribution coefficient:  $K_D$  and the related retardation coefficient:  $R_D$ ) and mobility of  
86 contaminants for solid-phase soil and aquifer materials. Both methods have strengths and  
87 weaknesses. Batch experiments represent the simplest means to test analyte sorption, but these  
88 experiments are static, and equilibrium oriented; questions about the applicability of the results to  
89 natural systems with flowing water and potentially changing levels of saturation logically persist  
90 (Schlüter et al., 1995 Schlüter, 1997; Van Glubt et al., 2022). Flow-through columns provide a much  
91 more dynamic and manipulatable experimental environment that is also not exclusively limited to  
92 equilibrium-based sorption simulations. Nonetheless, they are more laborious, difficult to replicate  
93 from column to column, column boundaries (walls) can present preferential flow problems, and  
94 despite the ability to manipulate the physicochemical properties of the columns this inevitably  
95 underrepresents the inherent variability of actual soil/aquifer conditions (Sentenac et al., 2001;  
96 USEPA, 2004). Soil contaminant transport modelling is a rapidly developing field of research and  
97 provides an alternative/complementary method to these traditional experimental methods. While  
98 Hg soil transport modelling is also advancing, progress is somewhat limited by the lack of  
99 measurement data particularly relating to  $K_D$  values, Hg speciation and methods of assessing specific  
100 processes for different soil/solid-phase materials (Leterme et al., 2014; Richard et al., 2016a).

101 Thus, it is important from both experimental and modelling standpoints that we determine effective  
102 means of deriving information on sorption/mobility of Hg in soils. Lacking the capacity to measure  
103 aquifer systems *in-situ*, we deem column experiments using solid-phase materials sourced from

104 sites of interest as the best available method to do so. Within this study, we aim to determine the  
 105 sorptive (and desorptive) capacity of low OM aquifer materials for Hg(II) using column experiments  
 106 and total Hg (THg) concentration, speciation, and stable isotope analyses of both solid and liquid-  
 107 phase materials. These experiments will be the first conducted on such low OM soil/aquifer material  
 108 and provide critical data into Hg transport and sorption within low OM soil and aquifer systems to  
 109 improve our geochemical understanding of subsurface Hg behaviour and for soil chemistry and  
 110 transport modelling. In addition, these column experiments on uncontaminated aquifer material  
 111 sourced from an area adjacent to a former industrial site at which HgCl<sub>2</sub> was applied as wood  
 112 preservative will simulate the contamination process. Data will aid our interpretation of the Hg  
 113 biogeochemistry in coupled soil-groundwater systems, as well as future Hg groundwater transport  
 114 modelling, and potentially provide guidance on contaminated site remediation.

## 115 2 Methods

### 116 2.1 Materials and experimental setup

117 The solid-phase material used in these experiments is highly permeable sand-gravel sediments  
 118 sourced from the saturated zone of an unconsolidated aquifer (approximate depth: 10 m) extracted  
 119 by a soil drill core in 2019. This site was impacted by losses of approximately 10-20 tonnes of Hg in  
 120 the form of high concentration HgCl<sub>2</sub> solution ( $\approx 0.66\%$  HgCl<sub>2</sub>) that was applied to timber as a  
 121 preservative (Schöndorf et al., 1999; Bollen et al., 2008; McLagan et al., 2022). The solid-phase  
 122 materials were extracted from outside of the plume of contaminated groundwater (Site B in  
 123 McLagan et al., 2022); and hence, the starting THg concentration within was very low (Table 1). The  
 124 geology and structure of the soil/aquifer profile has been described in detail in previous works  
 125 (Schöndorf et al., 1999; Bollen et al., 2008; McLagan et al., 2022). The material was stored in a dark  
 126 and cool place before drying at 30 °C for 48 hours. It was then sieved to a size of <2 mm using a  
 127 mesh soil sieve, which resulted in a distribution of  $74.1 \pm 4.6\%$  coarse load (>2 mm; not used) and  
 128  $25.8 \pm 4.6\%$  fine load (<2 mm). A subsequent particle size analysis of the fine load was carried out  
 129 using sieving and sedimentation method (DIN ISO 11277, 2002), and results (see Table 1) categorise  
 130 the solid-phase aquifer materials as a sandy-loam on the soil texture triangle. A summary of the  
 131 properties of the investigated material is shown in Table 1.

132 *Table 1: Properties of the solid-phase aquifer material used.*

Parameter	Fe (g kg <sup>-1</sup> )	Mn (mg kg <sup>-1</sup> )	Hg ( $\mu$ g kg <sup>-1</sup> )	TC (%)	TOC (%)	TIC (%)	Clay (%)	Silt (%)	Sand (%)
<b>Value</b>	19.2 $\pm$ 1.5	690 $\pm$ 160	20.4 $\pm$ 1.0	0.50 $\pm$ 0.03	0.16 $\pm$ 0.02	0.34 $\pm$ 0.03	13.5	23.2	63.3
<b>Samples (n)</b>	16	16	6	3	3	3	1	1	1

133

134 A set of preliminary experiments prior to experiment 1 (EXP1) and experiment 2 (EXP2) were run to  
 135 optimise packing methods, flow rates, stock solution concentration, and time the experiments  
 136 would take, and these are detailed in Section S1. Based on these preliminary data the experimental  
 137 setup was based on a modified version of DIN method 19528-01 (DIN 2009). 8 x 60 mL disposable  
 138 polypropylene syringes (height: 15.49 cm; inner diameter: 2.97 cm) were used as columns in each  
 139 experiment (Figure 1). The insides of the columns were roughened with sandpaper (and thoroughly  
 140 cleaned with surfactant and rinsed with deionised water to remove any debris) in order to minimise  
 141 preferential flow along the walls of the column. Each column was then filled with a layer of quartz  
 142 wool and a layer of quartz beads whose combined volume reached the 10 ml mark on the syringe.

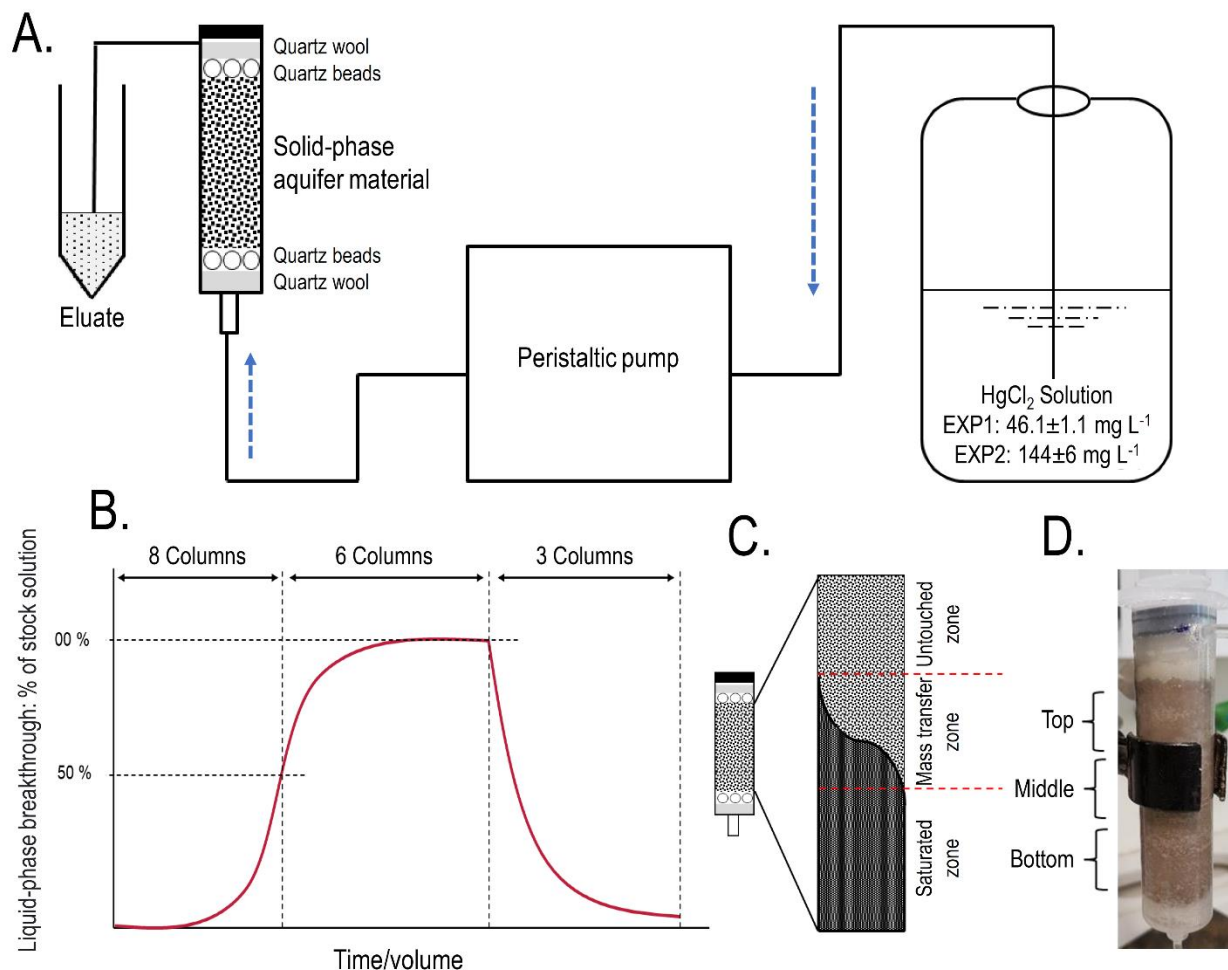
143 The sieved and dried material was then transferred by  $\approx 14$  g aliquots into the syringes (preliminary  
144 testing revealed dry packing achieved optimal column density and was best at preventing  
145 separation). Each aliquot was compacted to the desired volume and the surface of each aliquot was  
146 broken up before the addition of the subsequent aliquot to prevent layering between each addition.  
147 The mean mass and bulk density ( $\rho_b$ ) of the solid-phase aquifer materials added to the columns was  
148  $70.09 \pm 0.04$  g and  $1.42 \pm 0.01$  g cm<sup>-3</sup>, respectively, in EXP1, and  $70.05 \pm 0.03$  g and  $1.43 \pm 0.01$  g cm<sup>-3</sup>,  
149 respectively, in EXP2. This resulted in the height of the solid-phase materials within the column  
150 being  $\approx 11$  cm. Additional layers of quartz beads then quartz wool (syringe volume again  $\approx 10$  mL)  
151 were added on top of the solid-phase materials to reduce column separation and particle transport.  
152 Individual columns are named C1.1 to C1.8 for EXP1 and column C2.1 to C2.8 in EXP2. According to  
153 Lewis and Sjöström (2010), the average bulk densities range from 1.2 – 2.0 g cm<sup>3</sup> for sands and 1.6  
154 – 2.0 g cm<sup>3</sup> for gravel. Thus, we deem the achieved bulk density of the columns to be appropriate  
155 for these materials, particularly as densities of the removed coarse materials are higher (solid  
156 densities are estimated at 2.65 g cm<sup>3</sup>; Lewis and Sjöström (2010)).

157 All column experiments were conducted under saturated conditions. Figure 1A shows the  
158 configuration of the setup with the peristaltic pump upstream of the columns and flow through the  
159 columns was bottom to top to minimise entrapment of air and preferential flow paths. The stock  
160 solution, peristaltic pump, columns, and eluate sampling points were connected with 3.125 mm  
161 (inner-diameter) polypropylene tubing (length:  $105 \pm 10$  cm;  $n = 16$ ). To simulate the aquifer (flow  
162 velocity of  $\approx 3 - 10$  m day; Schöndorf et al., 1999; Bollen et al., 2008) and prevent separation of the  
163 solid-phase materials within the column, the lowest possible volume flow of  $0.62 \pm 0.02$  ml min<sup>-1</sup> ( $n$   
164 = 16) was set across all columns (flow velocities measured before and after experiments; Section  
165 S2). The stock solution was made using mixing HgCl<sub>2</sub> salt with tap water and stored in a 20 L  
166 polyethylene container. Tap water was selected due to its inherent concentration of ions, low  
167 potential for biological activity, and ease-of-use (challenges in extraction, storage, and transport of  
168 large groundwater volumes from study site  $\approx 600$  km away). Critically, the tap water and eluate DOC  
169 concentrations ( $2.3 - 3.3$  mg L<sup>-1</sup>) were of a similar range (even slightly less) than the values measured  
170 by Richard et al (2016a) at the site these solid-phase materials were removed ( $3.8 - 6.3$  mg L<sup>-1</sup>). This  
171 should eliminate the possibility that tap water would introduce a significant amount of artificial  
172 sorption sites associated with DOC being added to the system.

173 Stock solutions were  $46.1 \pm 0.1$  mg L<sup>-1</sup> in EXP1 ( $n = 6$ ) and  $144 \pm 6$  mg L<sup>-1</sup> in EXP2 ( $n = 12$ ) and were  
174 selected for (i) experimental constraints/time considerations (see Figure S1.6) and (ii) these values  
175 remain between HgCl<sub>2</sub> concentration applied during industrial activities ( $6600$  mg L<sup>-1</sup>; spillages of  
176 this solution to the top of the soil profile) and recently measured groundwater concentrations up to  
177  $164 \pm 75.4$   $\mu$ g L<sup>-1</sup> observed 55 years after cessation of the industrial activities at the site (McLagan  
178 et al., 2022). The physicochemical properties of both the stock solutions and eluate were monitored  
179 across the experiments and data are listed in Section S2. Desorption was performed by replacing  
180 the stock solution with tap water flowing at the same velocity. In total (sorption, equilibrium, and  
181 desorption), EXP1 and EXP2 ran continuously for 14 days, 3 hours, and 9 minutes, and 10 days, 13  
182 hours and 4 minutes, respectively.

183 Columns were pre-conditioned with tap water for 1 week at the experimental flow velocity to allow  
184 equilibration between the solid-phase materials and the dissolved substances in the tap water, the  
185 major component of the stock solution used within the experiment. After 24 hours of pre-  
186 conditioning, NaCl salt solution tracer experiments were conducted to monitor the rate of water

187 transfer through the columns (assuming NaCl is a conserved tracer that does not interact with the  
 188 solid-phase materials). The NaCl solution was passed into the system for 10 minutes and then  
 189 replaced with tap water. The change in conductivity was measured over time using a hand-held  
 190 electronic conductivity meter to produce NaCl (tracer) breakthrough curves. Results show good  
 191 column flow consistencies similar to the volumetric flow measurements and both data sets are  
 192 described in detail in Sections S1 and S2. The system was rigorously tested and checked for leaks  
 193 during both the pre-conditioning and testing phases.



194  
 195 *Figure 1: A. Schematic representation of the experimental setup. B. Theoretical model of the*  
 196 *experiments indicating sorption and desorption phases and column termination points for solid*  
 197 *phase analyses (2 columns terminated at 50 % breakthrough, 3 columns terminated at ≈equilibrium,*  
 198 *and the final 3 columns terminated after desorption; end of experiment). C. Representation of the*  
 199 *zones of mass transfer of Hg during the sorption phase (“saturated zone” refers to solid-phase in*  
 200 *that zone reaching its equilibrium uptake capacity for Hg at the experimental solution*  
 201 *concentration). The dark area describes the rising front of mercury. D. Allocation of column sections*  
 202 *(≈15 mL in each section) for solid-phase analyses (“Bottom” is the solution entry point).*

203 10 mL of eluate was allowed to flow off into a waste vessel before 5 mL of sample was collected for  
 204 analysis (this applied to all analyses). The liquid-phase was sampled for THg concentrations  
 205 consistently throughout the experiments: 38x in EXP1 (10x up to ≈50% breakthrough – columns  
 206 C1.1-C1.8; 11x between ≈50% breakthrough and ≈equilibrium – columns C1.1-C1.6; and 17x during  
 207 desorption – columns C1.1-C1.3) and 35x in EXP2 (8x up to ≈50% breakthrough – columns C2.1-C2.8;  
 208 16x between ≈50% and ≈100% breakthrough – columns C2.1-C2.3 and C2.6-C2.8; and 11x during

209 desorption – columns C2.1-C2.3). Liquid-phase speciation samples were collected 8x at ≈25%, 50%,  
210 75% breakthrough, and ≈equilibrium, at the end of the equilibrium (immediately before stock  
211 solution was changed to tap water), and ≈0% (immediately after stock solution was changed to tap  
212 water), 50% and at the end of desorption for both experiments. Liquid-phase stable isotope samples  
213 were collected only from columns C2.1-C2.3 in EXP2 9x in total. Collections were similar to liquid-  
214 phase speciation sampling points with an additional collection during the sorption stage of the  
215 experiment. After termination, solid-phase materials were analysed for THg concentrations, Hg  
216 species, and Hg stable isotopes. In summary, C1.7 and C1.8 and C2.4 and C2.5 were sacrificed at  
217 ≈50% breakthrough; C1.4-C1.6 and C2.6-C2.8 after equilibrium (≈100% breakthrough); while C1.1-  
218 C1.3 and C2.1-C2.3 went through to the end of desorption.

## 219 2.2 Analyses

### 220 2.2.1 Liquid-phase THg and speciation analyses

221 Eluate samples for THg and Hg stable isotope analyses were immediately stabilized by adding 1% by  
222 volume of 0.2 M bromine monochloride (BrCl) prepared according to Bloom et al. (2003). In order  
223 to break up all of the organically bound mercury in the liquid, a reaction time of the BrCl of 24-hours  
224 is recommended (US EPA method 1631, 2002). However, with little OM (Table 1), we assessed  
225 sample THg analysis only 1-hour after BrCl addition and there was no impact on sample recovery  
226 (Table S1.2). Immediately prior to analysis, hydroxylamine hydrochloride (NH<sub>2</sub>OH·HCl) was added to  
227 neutralize the BrCl followed by addition of tin(II) chloride (SnCl<sub>2</sub>) solution as the Hg reducing agent.

228 Liquid-phase speciation analyses followed the same methods described elsewhere (Bollen et al,  
229 2008; Richard et al., 2016b; McLagan et al., 2022). We describe this method as a complementary,  
230 semi-quantitative analytical tool and produces four distinct “fractions” of the total pool of liquid-  
231 phase Hg: (i) elemental Hg (Hg(0)) (purged from untreated eluate sample), (ii) dissolved inorganic  
232 Hg(II) termed Hg(II)A; (purged after reduction with SnCl<sub>2</sub> treatment; e.g. HgCl<sub>2</sub>); (iii) DOM-bound  
233 Hg(II) termed Hg(II)B (purged after BrCl and SnCl<sub>2</sub> treatment), and (iv) particulate Hg termed Hg(II)P  
234 (difference between THg concentrations in filtered and total unfiltered eluate samples). Both  
235 concentration and speciation results were measured using a cold-vapor atomic absorbance  
236 spectrometer (CV-AAS) (Hg-254 NE, Seefeldler Messtechnik GmbH, Germany) according to DIN  
237 method 1483 (2007) and USEPA method 1631 (2002). Confidence in liquid phase Hg(0)  
238 concentrations is higher than for other species, as these result from purging untreated/unstabilised  
239 samples of Hg(0) with nitrogen gas directly into the CV-AAS; all Hg(0) samples were analysed within  
240 30 mins of sample collection.

### 241 2.2.2 Solid-phase THg and speciation analyses

242 After individual columns were sacrificed for solid-phase analyses, the ends of the columns were  
243 sealed to prevent the columns from draining and stored in the same upright position as the  
244 experimental setup (Figure 1) to prevent further disturbance. Columns were cut into sections (Figure  
245 1D), homogenised and subset within 1 week of the end of the experiments and stored at 4°C in  
246 brown (opaque) falcon tubes until digestions or analyses. All analyses were performed on wet  
247 samples to minimise any potential losses of Hg(0). The moisture content of solid-phase samples was  
248 determined on separate aliquots for each column by difference after drying at 35 °C and was 23 ±  
249 2% (*n* = 48) (Section S8).

250 THg and Hg stable isotope analyses were cold digested in modified aqua regia following the methods  
251 described in McLagan et al. (2022) (8 mL HCl, 3 mL HNO<sub>3</sub>, and 1mL BrCl). Analyses of THg  
252 concentrations from the digestion extracts were determined using CV-AAS following DIN method  
253 1483 and USEPA method 1631. Results are reported on a dry weight basis and moisture content was  
254 determined by difference after baking at 105 °C using aliquots of the solid-phase sample (Section  
255 S8). Due to the low concentrations in the original solid-phase aquifer materials, THg concentrations  
256 were measured with a DMA80 (Milestone SCI) via thermal decomposition, amalgamation, and AAS  
257 (Table 1).

258 Speciation analyses were performed by pyrolytic thermal desorption (PTD), which continually  
259 measures Hg at 254 nm within an AAS detector that is connected to a sample combustion furnace  
260 that heats samples from room temperature to 650°C a 1°C per minute in a stream of N<sub>2</sub> gas. This  
261 method is described in detail by Biester and Scholz (1996). The sample release curves were  
262 compared to the release curves for a series of Hg reference materials (Hg(0), HgCl<sub>2</sub>, Hg<sub>2</sub>Cl<sub>2</sub> (calomel),  
263 cinnabar: α-HgS, metacinnabar: β-HgS, and Hg<sup>2+</sup>-sulphate: HgSO<sub>4</sub>) in silicon dioxide (SiO<sub>2</sub>) matrix  
264 (see Section S9 for reference material curves) to qualitatively assess the species or “fractions” of Hg  
265 present in the samples.

### 266 2.2.3 Liquid- and solid-phase Hg stable isotope analyses

267 Samples for stable Hg isotope analyses included stabilized liquid-phase eluate samples and solid-  
268 phase aqua-regia extracts diluted with deionised water (18.2 MΩ cm). Liquid-phase samples were  
269 collected in 15 mL polypropylene tubes and stabilized with BrCl to reach 1% of the sampled volume.  
270 Analyses were made using a Nu Plasma II (Nu Instruments) multicollector inductively coupled  
271 plasma mass spectrometer (MC-ICP-MS) with a cold-vapor generator (HGX-200; Teledyne Cetac)  
272 that allows direct addition of Hg(0) into MC-ICP-MS plasma by reducing all Hg in samples with SnCl<sub>2</sub>.  
273 The isotope ratios were determined relative to NIST-3133 (National Institute of Standards and  
274 Technology; NIST) using the standard bracketing approach and corrected for mass-bias using  
275 thallium (Tl) doping from NIST-997 (NIST) introduced using an Aridus-2 desolvating nebulizer  
276 (Teledyne CETAC). MDF was assessed by variation in δ<sup>202</sup>Hg, while Δ<sup>199</sup>Hg, Δ<sup>200</sup>Hg, Δ<sup>201</sup>Hg, and  
277 Δ<sup>204</sup>Hg were used to assess MIF of odd and even isotopes) (see Grigg et al., 2018; McLagan et al.,  
278 2022 for method details).

### 279 2.2.4 Complementary analyses

280 Metal cations in the solid- and liquid-phases were measured with inductively coupled plasma optical  
281 emission spectrometry (ICP-OES; Varian 715-ES; Agilent Technologies Inc.). Solid-phase total carbon  
282 (TC), total organic carbon (TOC), and total inorganic carbon (TIC; dissolved by hydrochloric acid)  
283 were measured by infra-red detection of CO<sub>2</sub> released (DIMA 1000NT; Dimatec, Germany).  
284 Dissolved organic carbon of stock solution and eluate was measured with a carbon/nitrogen  
285 analyser (Multi N / C 2100; Analytic Jena) (see Section S2). Liquid-phase dissolved oxygen content,  
286 redox potential, electrical conductivity, and pH were measured by handheld probes.

### 287 2.2.5 Retardation (R<sub>D</sub>) and sorption/partitioning/distribution (K<sub>D</sub>) coefficient calculations

288 The retardation coefficient (R<sub>D</sub>) is essentially the ratio of the velocity of the water front (v<sub>w</sub>) and  
289 velocity of the Hg front delayed by sorption processes (v<sub>Hg</sub>) moving through the columns (Equation  
290 1). Since the path of the the soluble pollutant (Hg) and water are the same, transport time can be  
291 determined based on the time it takes the fronts to pass through the columns (t<sub>Hg</sub> and t<sub>w</sub>,



292 respectively). NaCl breakthrough curve was used as a proxy for water based on the assumption it is  
293 a conservative tracer.  $t_{Hg}$  and  $t_w$  are given when the respective ratios of the NaCl and THg  
294 concentrations in the eluate is equal to half the input concentration (stock solution;  $C_{eluate} / C_{initial} =$   
295 0.5) (Patterson et al., 1993; Reichert, 1991; Schnaar and Brusseau, 2013).

$$296 \quad R_D = V_w / V_{Hg} = t_w / t_{Hg} \quad \text{Equation 1}$$

297  $R_D$  is related to the sorption or partitioning or distribution coefficient ( $K_D$ ; mL g<sup>-1</sup>) according to  
298 Equation 2 and Equation 3 (USEPA, 2004):

$$299 \quad R_D = 1 + (\rho_b / n_e) K_D \quad \text{Equation 2}$$

$$300 \quad K_D = (R_D - 1) (n_e / \rho_b) \quad \text{Equation 3}$$

301 Where,  $n_e$  is the effective porosity (EXP1:  $0.470 \pm 0.008$ ,  $n = 3$ ; EXP2:  $0.459 \pm 0.004$ ,  $n = 3$ ; assumed  
302 to be equal to total porosity), which is the ratio of the column pore volume (EXP1:  $23.3 \pm 0.5$  mL,  $n$   
303 = 3; EXP1:  $22.5 \pm 0.1$  mL,  $n = 3$ ) to the total volume of the solid-phase materials of the columns (EXP1:  
304  $49.7 \pm 0.3$  mL,  $n = 3$ ; EXP2:  $49.0 \pm 0.5$  mL,  $n = 3$ ).  $R_D$  could only be calculated for columns that went  
305 to equilibrium and desorption (not 50% breakthrough),  $n_e$  was calculated for columns that went  
306 through desorption (C1.1-C1.3 and C2.1-C2.3); and hence,  $K_D$  was only calculated for these columns.  
307 Note, the pore volumes reported above are the data used when reporting the number of pore  
308 volumes.

### 309 2.3 Quality Assurance and quality control (QAQC)

310 For liquid-phase analyses, a  $140.8 \text{ ng L}^{-1}$  Hg(II) stock solution (Sigma Aldrich) was measured  
311 throughout the analyses and recovery was  $99 \pm 5\%$  ( $n = 250$ ). For solid-phase analyses, Chinese Soil  
312 (NCS DC73030; Chinese National Analysis Centre for Iron and Steel) was measured and recovery was  
313  $101 \pm 6\%$  ( $n = 16$ ). The accuracy and precision of Hg stable isotope measurements was assessed  
314 using the “in-house” *ETH Fluka* standard. Mean values across the measurement sessions were:  
315  $\delta^{202}\text{Hg} = -1.42 \pm 0.08 \text{ ‰}$ ;  $\Delta^{199}\text{Hg} = 0.08 \pm 0.02 \text{ ‰}$ ;  $\Delta^{200}\text{Hg} = 0.02 \pm 0.02 \text{ ‰}$ ;  $\Delta^{201}\text{Hg} = 0.03 \pm 0.03 \text{ ‰}$ ;  
316  $\Delta^{204}\text{Hg} = -0.01 \pm 0.06 \text{ ‰}$  ( $n = 26$ ; all uncertainty values are reported as 2SD). All uncertainties are  
317 1SD, unless otherwise reported (i.e., 2SD used to report Hg stable isotope analysis uncertainty).  
318 These values are within the range of other studies (i.e., Obrist et al., 2017; Goix et al., 2019; McLagan  
319 et al., 2022). Theoretical solid-phase THg concentration (compared to measured THg  
320 concentrations) are determined via mass balance of liquid-phase THg concentrations of stock  
321 solution and eluate and the volume of stock solution applied to the columns. All statistical tests and  
322 sorption fitting comparisons were performed in OriginPro 2018 (Origin Lab Corporation).

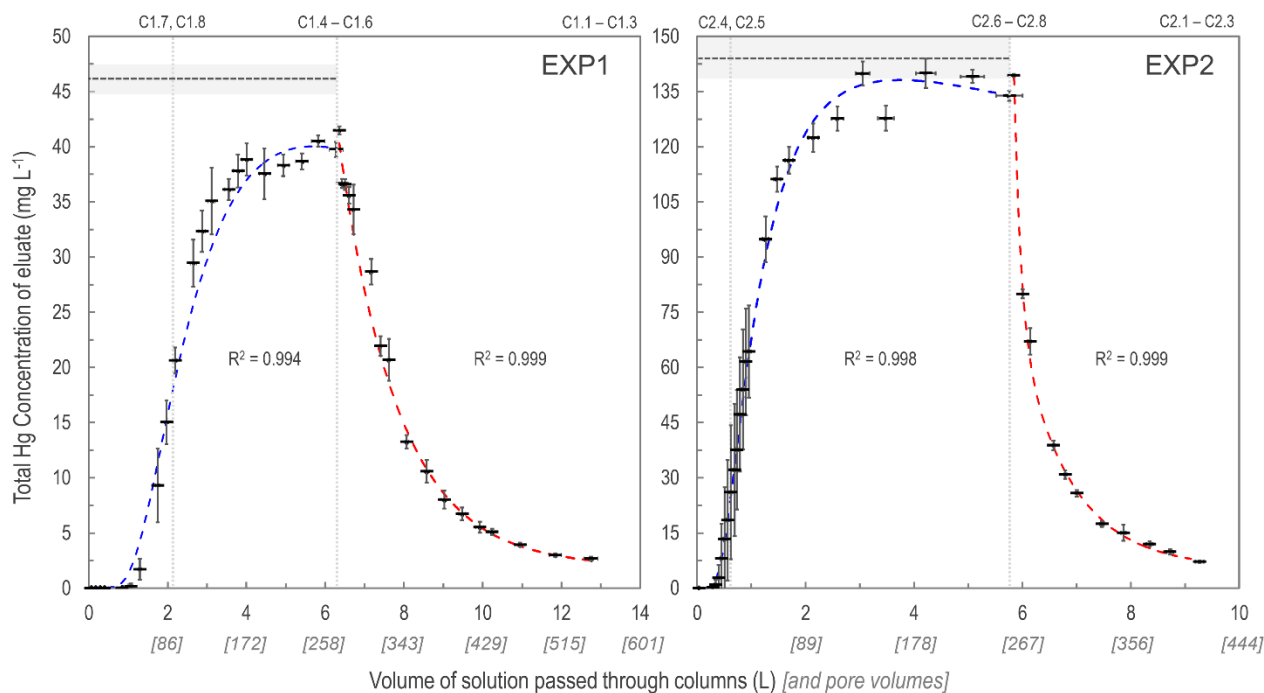
## 323 3 Results and discussion

### 324 3.1 Sorption and desorption behaviour of mercury in column experiments

#### 325 3.1.1 Sorption

326 As expected, the uptake of the HgCl<sub>2</sub> solution to the solid phase aquifer materials followed an *S-*  
327 *shaped* breakthrough curve best described by a Freundlich function (Figure 2; note these are  
328 empirically fitted functions). Initially, >99.9% of the Hg in solution was sorbed to the solid phase  
329 materials and 1.0-1.3 L (43 – 55 pore volumes) and 0.3-0.45 L (13 – 16 pore volumes), in EXP1 and  
330 EXP2, respectively, was required to reach eluate THg concentrations equivalent to 1% of stock

331 solution (Section S5). This was followed by a phase of rapid increase in the eluate concentrations  
 332 (decreasing fraction of the Hg in solution sorbing to the solid-phase). Finally, the increase in eluate  
 333 THg concentration slowed as it approached the upper asymptotic bound of the original stock  
 334 solution concentration in each experiment and equilibrium of Hg fluxes between the solid- and  
 335 liquid-phases was approached/reached. EXP1 likely did not completely reach a stable equilibrium  
 336 point (eluate concentration was at  $\approx 91\%$  of stock solution concentration when the stock solution  
 337 was changed to water), and more time/volume of solution was required. This would have required  
 338 creation of more stock solution; instead, green chemistry prevailed, and the choice was made to  
 339 move onto the desorption phase with consideration of the higher concentration (faster) follow-up  
 340 EXP2.



341

342 *Figure 2: Total Hg concentration eluate breakthrough curves for low (EXP1; left panel) and high*  
 343 *(EXP2; right panel) concentration stock solution experiments. Horizontal dashed lines (mean) and*  
 344 *shaded area (1SD) indicate the original stock solution concentrations in each experiment and vertical*  
 345 *dotted lines indicate column removal points (column IDs above panels indicate which columns were*  
 346 *removed). Uncertainty in the x-axis relates to the differing volumes passed through individual*  
 347 *columns at each sampling period. Sorption curves were fitted with Freundlich functions (blue dashed*  
 348 *lines), and desorption curves were fitted with exponential decay functions (red dashed lines). These*  
 349 *functions were empirically (not mechanistically) fitted to the data as these plots are not sorption*  
 350 *isotherms (see Section S6 for details of fitting functions).*

351 This S-shaped sorption behaviour was similar to the one other detailed study on Hg sorption in  
 352 natural soils with sufficient liquid-phase sampling frequency to create column breakthrough curves  
 353 on OM-rich (9.4 – 24.7% OM) Amazonian soils and similar stock solution concentrations (60 – 120  
 354  $\text{mg L}^{-1}$ ; Miretzky et al., 2005). Semi-quantitative liquid-phase Hg speciation analyses confirm that  
 355 the majority of Hg was dissolved inorganic Hg(II) (EXP1:  $83 \pm 6\%$ ; EXP2:  $77 \pm 8\%$ ), a fraction of which  
 356 will be soluble  $\text{HgCl}_2$  (species used to generate stock solution), but also fractions of hydrolysed  
 357 species (i.e.,  $\text{HgClOH}$ ,  $\text{Hg}(\text{OH})_2$ ,  $[\text{HgCl}_3]^-$ ) formed in solution at pH in the observed range (7.7 – 8.1)  
 358 of these experiments (Delnomdedieu et al., 1992; Gunneriusson and Sjöberg, 1992; Kim et al., 2004;  
 359 see also Section S10 for theoretical Hg speciation results using Visual MINTEQ v3.1). These liquid-

360 phase Hg speciation results are similar to those reported for groundwater samples previously  
361 collected at the contaminated site where these materials were extracted from (Bollen et al., 2008;  
362 Richard et al., 2016a; McLagan et al., 2022).

363 Despite the very low OM content (Table 1) within these solid-phase aquifer materials, the  
364 equilibrium uptake capacity was very high in both experiments. These concentrations were  
365 determined both (i) analytically by solid-phase THg analyses, and (ii) theoretically, based on the  
366 inverse of the breakthrough curve integral: the area above the curve and below the stock solution  
367 concentration. This has been referred to as “holdup” ( $H$ ; mg of Hg), (Van Genuchten and Parker,  
368 1984) and is described in Equation 4:

$$369 \quad H = [C_0 V_f - \int C_e dV] \quad \text{Equation 4}$$

370 Where,  $C_e$  is the eluate THg concentration ( $\text{mg L}^{-1}$ ),  $C_0$  is the stock solution THg concentration ( $\text{mg}$   
371  $\text{L}^{-1}$ ), and  $V_f$  is the accumulated solution volume that has passed through the columns at the point  
372 they were removed (L). Theoretical concentrations reached  $1880 \pm 20 \text{ mg kg}^{-1}$  in EXP1 and  $2810 \pm$   
373  $40 \text{ mg kg}^{-1}$  in EXP2 (Table 2; Section S3). These data are directly comparable, and indeed within the  
374 same range as the theoretical solid-phase concentrations calculated by Miretzky et al. (2005) for the  
375 OM-rich Amazonian soils (THg concentrations:  $950 - 3960 \text{ mg kg}^{-1}$ ). The elevated Hg sorption  
376 observed by Miretzky et al. (2005) is to be expected due to the affinity of Hg for OM (e.g., Yin et al.,  
377 1996; Jiskra et al., 2015; Manceau and Nagy, 2019). Nonetheless, Miretzky et al. (2005) found their  
378 calculated solid-phase THg concentrations at equilibrium (sorptive capacity of the soils) were  
379 greater when OM% + clay% was considered rather than OM% alone was considered (Miretzky et al.,  
380 2005), which highlights the potential role clay (and oxide) minerals can play in Hg sorption to solid-  
381 phase soil or aquifer materials.

382 Hg sorption to OM has been observed to increase at lower pH (Andersson, 1979; Yin et al., 1996).  
383 However, the opposite has been reported for sorption of Hg to clay minerals: in neutral and slightly  
384 basic soils, the sorption capacity is controlled by the mineral components (Andersson, 1979;  
385 Schuster, 1991; Gabriel and Williamson, 2004). Indeed, the pH range of the eluate and stock solution  
386 (pH range: 7.7 – 8.1) present ideal conditions for Hg sorption to clay minerals and Fe and Mn  
387 (oxy)hydroxide minerals. Hg sorption to these inorganic minerals becomes more likely in our  
388 experiments considering the very low OM content of the solid-phase materials (Table 1). Haitzer et  
389 al. (2002) estimated that at ratios of THg-to-OM above  $1 \mu\text{g}$  of Hg per mg of OM the strong thiol-  
390 group bonding sites for Hg within OM are saturated. Based on the TOC data of these solid-phase  
391 materials (assuming 0.16% TOC = 0.32 % OM), there would be 224 mg of OM within a column. To  
392 surpass the ratio of  $1 \mu\text{g}$  of Hg per mg of OM, only 4.9 and 1.6 mL of stock solution or 0.21 and 0.07  
393 pore volumes in EXP1 and EXP2, respectively, would need to be added to the columns to saturate  
394 the strong thiol-group binding sites with Hg. Considering that Hg breakthrough occurred only after  
395 about 50 and 15 pore volumes in EXP1 and EXP2, respectively, it can be assumed that not only the  
396 strong Hg-binding thiol-groups but also the other less strong Hg-binding functional groups (e.g.,  
397 carboxyl groups) of the small OM pool in the columns were fully saturated early in the experiments.  
398 Hence, solid-phase sorption of Hg within these experiments was dominated by interactions with  
399 inorganic minerals. The role of such inorganic minerals was also highlighted in one of the few studies  
400 that exist examining Hg transport and fate in aquifers (Lamborg et al., 2013).

401 *Table 2: Theoretical (liquid-phase THg mass-balance) and measured solid-phase THg concentrations*  
 402 *and recovery of the measured-to-expected (theoretical) concentrations for each the columns in EXP1*  
 403 *and EXP2.*

Experiment 1 (EXP1; $46.1 \pm 1.1 \text{ mg L}^{-1}$ )					Experiment 2 (EXP2; $144 \pm 6 \text{ mg L}^{-1}$ )				
Column	Stage	Theoretical Hg conc. ( $\text{mg kg}^{-1}$ )	Measured Hg conc. ( $\text{mg kg}^{-1}$ )	Recovery	Column	Stage	Theoretical Hg conc. ( $\text{mg kg}^{-1}$ )	Measured Hg conc. ( $\text{mg kg}^{-1}$ )	Recovery
C1.1	Desorption	820	$722 \pm 91$	88.0%	C2.1	Desorption	1360	$1060 \pm 230$	78.3%
C1.2	Desorption	890	$877 \pm 206$	98.6%	C2.2	Desorption	1300	$786 \pm 390$	60.2%
C1.3	Desorption	847	$835 \pm 120$	98.6%	C2.3	Desorption	1490	$1050 \pm 57$	70.1%
C1.4	Equilibrium	1870	$1470 \pm 221$	78.5%	C2.4	50% breakthrough	1030	$785 \pm 220$	76.1%
C1.5	Equilibrium	1910	$1630 \pm 286$	85.1%	C2.5	50% breakthrough	1140	$702 \pm 330$	61.4%
C1.6	Equilibrium	1870	$1440 \pm 92$	77.1%	C2.6	Equilibrium	2770	$2380 \pm 452$	86.1%
C1.7	50% breakthrough	1320	$1470 \pm 384$	111.3%	C2.7	Equilibrium	2850	$2320 \pm 388$	81.2%
C1.8	50% breakthrough	1300	$960 \pm 524$	73.6%	C2.8	Equilibrium	2820	$2260 \pm 272$	79.8%

404

405 Measured THg concentrations were typically lower than the theoretical calculated values (Table 2)  
 406 and contaminant masses can be difficult to balance in contaminant batch and column experiments  
 407 (Van Genuchten and Parker, 1984; Hebig et al., 2014). This is of particular concern for a contaminant  
 408 such as Hg whose stability and contamination issues have been widely studied due to the capacity  
 409 of different Hg species to sorb to and diffuse through plastic polymers (at differing rates) (Hall et al.,  
 410 2002; Parker and Bloom, 2005; Hammerschmidt et al., 2011). Loss of a fraction of the THg in solution  
 411 to/through tubing and the walls of the column is likely contributing to the lower recovery in some  
 412 of these samples. Other factors that could be contributing to the differences between the  
 413 theoretical and measured concentrations are heterogeneity of the solid-phase and solid-phase  
 414 sample extraction (particularly during movement of the Hg mass transfer front), loss of Hg from  
 415 solid-phase before sample extraction and analyses (particularly for volatile Hg(0); Parker and Bloom,  
 416 2005), and inherent analytical uncertainties. The heterogeneity of the materials is emphasized by  
 417 the absence of trends in THg concentrations within the sections of the columns, even for the  
 418 columns undergoing movement of the mass transfer zone (see Section S8). Unfortunately, Miretzky  
 419 et al. (2005) did not provide total sampling volumes for their experiments and no assessment of  
 420 measured THg recoveries was (or can be) made for direct comparison to our recovery data.

### 421 3.1.2 Desorption

422 The desorption phase of both EXP1 and EXP2 followed an exponential decay model; results confirm  
 423 that sorption is (partially) reversible and initially rapid (Figure 2). After the stock solution was  
 424 switched to water for the desorption phase, the eluate solution reached <50% of the stock solution  
 425 THg concentration with additions of  $\approx 1 \text{ L}$  ( $\approx 43$  pore volumes) and  $\approx 0.5 \text{ L}$  ( $\approx 22$  pore volumes) of  
 426 solution in EXP1 and EXP2, respectively (Figure 2). At the termination of the experiments eluate THg  
 427 concentrations dropped to <10% of the original stock solution (Figure 2). While it is evident that  
 428 more Hg would have been released if desorption was permitted to proceed further (terminated due  
 429 to time and to prevent excess contaminated waste solution), measured data indicated that  $46 \pm 6\%$   
 430 (Theoretical:  $55 \pm 2\%$ ) in EXP1 and  $58 \pm 10\%$  (Theoretical:  $51 \pm 4\%$ ) in EXP2 of THg could be extracted  
 431 from the solid-phase materials before the experiments were terminated. Evidence from the  
 432 contaminated aquifer where these solid-phase materials were extracted suggest that the retention  
 433 of a fraction of this Hg within the solid-phase materials is long-term (Bollen et al., 2008; McLagan et

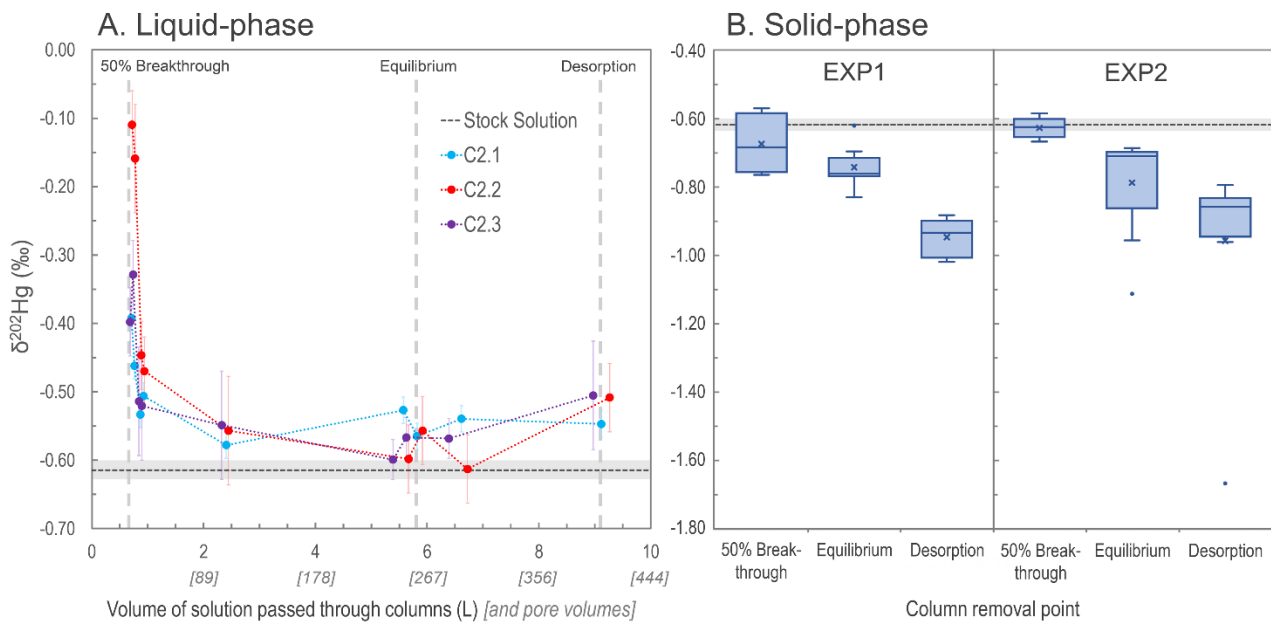
434 al., 2022). McLagan et al. (2022) report that elevated solid- (up to 562 mg kg<sup>-1</sup>) and liquid-phase (up  
435 to 164 ± 75.4 µg L<sup>-1</sup>) THg concentrations are still found at the site to the present day, more than 55  
436 years since the industrial use of Hg (kyanisation) at the site ceased.

437 McLagan et al. (2022) associate this residual retention of Hg to the diffusion of Hg into the mineral  
438 matrix or secondary transformation to a more stable (and less soluble) Hg(II) species (McLagan et  
439 al., 2022). Previous work agrees that sorption and subsequent release of Hg to/from solid-phase  
440 soils and solid-phase materials is likely controlled by multiple processes (Yin et al., 1997; Bradl, 2004;  
441 Reis et al., 2016). The more easily extractable Hg is likely to be associated with Fe and Mn  
442 (oxy)hydroxide, and clay minerals through outer-sphere complexes that form through cation  
443 exchange and electrostatic intermolecular forces (Bradl, 2004; Reis et al., 2016). Over time, some of  
444 the Hg associated through these weaker surface interactions will diffuse into the matrix and/or form  
445 inner-sphere complexes, processes that both slow the release of the sorbed Hg (Bradl, 2004; Reis et  
446 al., 2016). Similar results were observed by Miretzky et al. (2005) in the OM rich Amazonian soil  
447 columns with 27 - 38% of Hg sorbed to the solid-phase materials being rapidly redissolved in the  
448 initial desorption phase. However, the soils with higher OM content showed stronger hysteresis and  
449 considerably less Hg was released during the second phase of desorption (Miretzky et al., 2005) than  
450 in our low OM solid-phase materials suggesting stronger interactions of inner-sphere complexed Hg  
451 with OM; results supported by work done in other studies examining Hg sorption to solid-phase  
452 materials (Yin et al., 1996; Reis et al., 2016).

### 453 3.1.3 Insights from stable Hg isotopes

454 Variations in δ<sup>202</sup>Hg values, describing MDF of Hg isotopes, were observed in both the liquid- and  
455 solid-phase across the experiments (Figure 3; Section S7; Section S8). During the initial phase of the  
456 experiments (before eluate breakthrough), transfer of Hg from the applied stock solution  
457 (δ<sup>202</sup>Hg: -0.61 ± 0.01‰ relative to NIST-3133, 1SD; n = 3) to the solid-phase materials is complete.  
458 When there is complete transfer of a “pool” of Hg from reactants to products there is complete  
459 transfer of stable isotopes; and hence no fractionation can be observed.

460 Once Hg begins to breakthrough the columns, the eluate is initially enriched in heavy isotopes  
461 associated with the preferential transfer (sorption) of lighter isotopes to the solid-phase materials  
462 (Jiskra et al., 2012; Wiederhold, 2015) with heavier isotopes retained in solution (passed into the  
463 eluate). In all three of the EXP2 columns examined for stable isotopes in the liquid-phase, the first  
464 two liquid-phase stable isotope samples (sampled just after ≈50% breakthrough column removals)  
465 had more positive δ<sup>202</sup>Hg values than the remaining liquid-phase samples (Figure 3). However, it is  
466 also apparent that at ≈50% breakthrough, there was little MDF imparted on the solid-phase  
467 materials compared to the stock solution (Figure 3). This ostensibly contrasting finding (observable  
468 positive MDF in the liquid-phase and little negative MDF in the solid-phase) can be explained by the  
469 proportion of Hg transferred to the solid-phase of the total mass added in solution. At the 50%  
470 breakthrough column removal, the proportion of Hg sorbed by the columns was 95.4 and 90.4%,  
471 respectively for C1.7 and C1.8 (EXP1) and 83.8 and 88.5%, respectively for C2.4 and C2.5 (EXP2;  
472 based on theoretical calculations). The majority of this sorption occurred during the complete (or  
473 near-complete) transfer of isotopes before (or just after) eluate breakthrough. Hence, the MDF that  
474 began to occur after breakthrough (observable in the early liquid-phase eluate samples) had little  
475 influence on the Hg stable isotope ratios of the solid-phase materials of columns removed at the  
476 ≈50% breakthrough point.



477

478 *Figure 3: Development of liquid-phase  $\delta^{202}\text{Hg}$  values for columns C2.1 – C2.3 measured at nine*  
 479 *intervals during EXP2 (Panel A). Box plots of solid-phase  $\delta^{202}\text{Hg}$  values measured in both EXP1 and*  
 480 *EXP2 (“x” denotes mean values, dots denote outliers) (Panel B). In both panels, the grey dash line*  
 481 *represents the mean  $\delta^{202}\text{Hg}$  value (light grey rectangle: 1SD) measured for the stock solution. Note,*  
 482 *the vertical grey dashed lines indicating solid-phase column removal points in the left panel are only*  
 483 *approximations as the liquid-phase stable isotope measurements were only made on columns C2.1-*  
 484 *2.3 that proceeded until the end of desorption.*

485 This finding of limited MDF on solid phase materials at  $\approx 50\%$  breakthrough is consistent with the  
 486  $\delta^{202}\text{Hg}$  values observed within the column layers. The bottom layers of C1.7 ( $\delta^{202}\text{Hg}$ :  $-0.76 \pm 0.07\text{‰}$ )  
 487 and C1.8 ( $\delta^{202}\text{Hg}$ :  $-0.75 \pm 0.07\text{‰}$ ) in EXP1 were more negative than the stock solution, while the top  
 488 layers ( $\delta^{202}\text{Hg}$ :  $-0.57 \pm 0.15\text{‰}$  and  $\delta^{202}\text{Hg}$ :  $-0.59 \pm 0.07\text{‰}$  for C1.7 and C1.8, respectively) were  
 489 equivalent to the stock solution (Section S8). These data suggest observable MDF was beginning to  
 490 occur in the part of the column exposed to the Hg front (bottom) for the longest. The same was not  
 491 the case in EXP2 (no observable trend in  $\delta^{202}\text{Hg}$  between layers; Section S8). We attribute this to the  
 492 more elevated THg concentrations and faster movement of the Hg front moving through the  
 493 columns (see Table 3 below) in EXP2 overwhelming the layering MDF observed in EXP1.

494 As sorption progresses to equilibrium, we observe a negative shift in the eluate  $\delta^{202}\text{Hg}$  value of all  
 495 three columns falling in the range of  $\approx -0.6$  to  $-0.5\text{‰}$ , which is slightly more positive than the stock  
 496 solution ( $\delta^{202}\text{Hg}$ :  $-0.61 \pm 0.01 \text{‰}$  1SD;  $\pm 0.08 \text{‰}$  analytical 2SD; Figure 3). During this transition in the  
 497 Hg uptake process the net effect is that most, and then essentially all, Hg input from the stock  
 498 solution is passing through the columns and into the eluate and any kinetic MDF occurring would  
 499 be limited. Nonetheless, equilibrium-based isotope exchange would also drive lighter isotopes into  
 500 the solid-phase materials (Wiederhold et al., 2010; Jiskra et al., 2012; Wiederhold, 2015), which is  
 501 the likely explanation for the liquid-phase  $\delta^{202}\text{Hg}$  values remaining slightly more positive than the  
 502 stock solution. While the impact of this MDF on the continuously flowing eluate is small when the  
 503 system is at equilibrium, the effect of this equilibrium-based MDF on the solid-phase is more  
 504 manifest as its effect is cumulative. Over time, more and more lighter isotopes preferentially sorb  
 505 to the solid-phase; and hence, the mean  $\delta^{202}\text{Hg}$  values of the solid-phase materials in EXP1  
 506 ( $\delta^{202}\text{Hg}$ :  $-0.74 \pm 0.06\text{‰}$  1SD) and EXP2 ( $\delta^{202}\text{Hg}$ :  $-0.79 \pm 0.15\text{‰}$  1SD) at the end of the sorption

507 experiments (at or near column equilibrium) are more negative than the stock solution (and solid-  
508 phase materials at  $\approx 50\%$  breakthrough). Thus, we suggest equilibrium-based MDF (with some  
509 potential for kinetic MDF contributions) to be the primary driver of the more negative  $\delta^{202}\text{Hg}$  values  
510 observed in the solid-phase materials at the end of the equilibrium-phase of the experiments. These  
511 observations agree with the observed results of McLagan et al. (2022) sampled within the  
512 contaminated aquifer adjacent to which these uncontaminated materials were derived.

513 At the end of the desorption phase, the solid-phase materials have undergone further MDF to more  
514 negative  $\delta^{202}\text{Hg}$  values (EXP1  $\delta^{202}\text{Hg}$ :  $-0.95 \pm 0.05\%$ ; EXP2  $\delta^{202}\text{Hg}$ :  $-0.96 \pm 0.27\%$  1SD). Two of the  
515 three columns monitored for liquid-phase stable isotopes at the end of desorption also show a slight  
516 positive MDF shift and values for all three columns are slightly more positive ( $\delta^{202}\text{Hg}$ :  $-0.55$  to  $-0.51$   
517  $\%$ ) than the stock solution (Figure 3). As discussed, desorption proceeds via a two-step mechanism:  
518 a rapid initial desorption as easily exchangeable, outer-sphere complexed Hg is released, followed  
519 by a slower phase of desorption as this easily exchangeable pool depletes. Broczka et al. (2019) and  
520 McLagan et al. (2022) suggest that this easily exchangeable pool is enriched in heavier isotopes  
521 compared to the fraction that diffuses into the mineral matrix or transforms to more stable, less  
522 soluble Hg(II) species as these secondary processes favour lighter isotopes. Thus, removal of the  
523 heavy isotope enriched, easily exchangeable pool of Hg is the likely driver of more negative  $\delta^{202}\text{Hg}$   
524 values in the solid-phase materials after desorption. While Demers et al. (2018) studied  
525 predominantly surface water samples linked to Hg soil-groundwater contamination at a site in  
526 Tennessee, USA (industrial use of Hg(0)), they did observe more positive  $\delta^{202}\text{Hg}$  values with elevated  
527 dissolved THg concentrations values in samples from the hyporheic zone associated with exfiltrating  
528 groundwater from the contaminated areas. These data would agree with the more positive liquid-  
529 phase  $\delta^{202}\text{Hg}$  values observed in our study and by McLagan et al. (2022).

530 Variation in both odd- and even-isotope MIF was within the range of analytical uncertainties  
531 (Section S7; Section S8). McLagan et al. (2022) did observe small variation in  $\Delta^{199}\text{Hg}$  between solid-  
532 and liquid-phases, which the authors suggest may be linked to MIF driven by dark abiotic reduction  
533 of Hg(II) (Zheng and Hintelmann, 2010). However, it is unlikely that this process could manifest into  
534 an observable change in  $\Delta^{199}\text{Hg}$  considering the short duration of these experiments even if the  
535 process could occur at all within these columns.

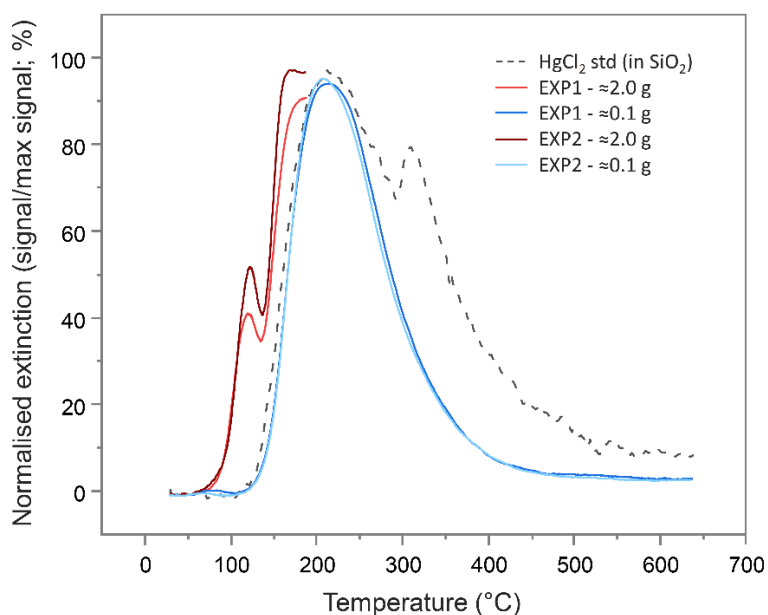
### 536 3.2 Is reduction of Hg(II) to Hg(0) occurring within the columns?

537 Reduction of Hg(II) to Hg(0) has been observed previously at this and other sites impacted by  
538 kyanisation activities (Bollen et al., 2008; Richard et al., 2016a; 2016b; McLagan et al., 2022). In  
539 these subsurface environments with low OM and very high THg concentrations, this secondary Hg(0)  
540 production has been linked to abiotic, (hydr)oxide mineral surface catalysed reactions driven by  
541 other redox active metals (Bollen et al., 2008; Richard et al., 2016a; 2016b; Schwab et al., 2023).  
542 Since  $\text{HgCl}_2$  solution was the only form of Hg applied in the column experiments, the presence of  
543 Hg(0) in either the liquid- or solid-phases must be explained via reduction of Hg(II).

544 To examine the presence of Hg(0), PTD analyses were run on the (undried) solid-phase materials  
545 from the columns after the sorption experiments. The PTD extinction curves showed little variation  
546 across all sections of all columns from either experiment (see Section S9). All curves mimic the low  
547 sample weight ( $\approx 0.1$  g) mean extinction curves displayed in Figure 4 and are dominated by a single  
548 peak with a maximum release of  $\approx 225$  °C, which aligns with the maximum extinction of the  $\text{HgCl}_2$   
549 standard in silicon dioxide ( $\text{SiO}_2$ ). This supports the hypothesis of direct (outer-sphere) complexation

550 or electrostatic interaction of dissolved Hg(II) species to the mineral surfaces posited previously  
551 (Bradl, 2004; Reis et al., 2016) and by McLagan et al. (2022). Nonetheless, these low sample weight  
552 PTD curves were indicative of some qualitative evidence of very small peaks at <175 °C (Section S9);  
553 peaks in this range are associated with Hg(0) (Biester and Scholz, 1996; McLagan et al., 2022). The  
554 initial sample masses used in the PTD analyses were low ( $\approx 0.1$  g) so as to not overwhelm the AAS  
555 detector, release large amounts of gas-phase Hg(0), and potentially cause memory effects in future  
556 analyses. Nevertheless, this would not occur if sample masses were increased ( $\approx 2.0$  g) and the  
557 temperature ramp stopped at  $\approx 175$  °C. When the solid-phase materials were analysed in this  
558 manner, Hg(0) peaks were detected across all sections of all columns in both experiments (see  
559 Section S9; Figure 4).

560 Additionally, detectable concentrations of Hg(0) were observed across all of the semi-quantitative  
561 liquid-phase Hg speciation analyses and elevated above the Hg(0) concentrations measured in the  
562 stock solution (Section S4). The observed liquid-phase fraction of Hg(0) was highest at the  $\approx 25\%$   
563 breakthrough sample collection point in EXP1 (0.7%) and EXP2 (0.1%) with the fraction being  $\leq 0.1\%$   
564 in all other samples (Section S4). While these data suggest that reduction of Hg(II) to Hg(0) begins  
565 almost immediately after the introduction of the HgCl<sub>2</sub> solution, we link the declining proportion of  
566 Hg(0) to the low solubility of Hg(0) ( $\approx 50$   $\mu\text{g L}^{-1}$ ) (Skylberg, 2012; Brocza et al., 2019), which was  
567 already reached at the  $\approx 25\%$  breakthrough sample collection point in both experiments.



568

569 *Figure 4: Mean pyrolytic thermal desorption (PTD) extinction curves from solid-phase materials from*  
570 *EXP1 and EXP2 assessed with two different sample masses. Analyses of the larger sample mass ( $\approx 2.0$*   
571 *g of material) were terminated when the temperature ramp reached  $\approx 175$  °C to prevent excessive*  
572 *gas-phase Hg release and potential memory effects on the instrument.*

573 These measured Hg(0) fractions in solid- and liquid-phase analyses provide further direct evidence  
574 of Hg(0) production under saturated, oxic conditions in low OM solid-phase materials. Hg(0)  
575 production in these contaminated aquifers has been linked to the slower than expected horizontal  
576 progress of the plume of Hg in the aquifer at the site where this contamination occurred (Bollen et  
577 al., 2008; Richard et al., 2016a; 2016b; McLagan et al., 2022). While these data indicate that the  
578 fraction of Hg(0) produced is relatively small, the volume of soil and aquifer materials in which this  
579 process can occur is large. The contamination plume of the aquifer at the site where the solid phase



580 materials were removed from is  $\approx 1000$  m long and covers an area of  $\approx 6 \times 10^4$  m<sup>2</sup> (Bollen et al., 2008;  
 581 McLagan et al., 2022). If we assume conservative values for mean depth of contamination of 2 m  
 582 (aquifer  $\approx 3$ -4 m depth; Bollen et al., 2008; McLagan et al., 2022), mean THg concentration of 2 mg  
 583 kg<sup>-1</sup> (solid phase THg concentration of 2-162 mg kg<sup>-1</sup> along the contaminated aquifer; Bollen et al.,  
 584 2008), the fraction of Hg(0) produced per day is 0.01 – 0.001% of the THg (based off 0.1% Hg(0) peak  
 585 integration of total peak area of mean PTD curve from EXP2; see Section S9)), and the same bulk  
 586 density and flow rates as in our experiments, we can produce a *back-of-the-envelope* estimate of  
 587 the mass of Hg(0) produced and potentially lost from the aquifer to overlying soils. Based off these  
 588 numbers, we estimate that 0.3 – 0.4 g of Hg(II) is transformed to Hg(0) each day within the aquifer  
 589 of the contaminated site in southern Germany; over the course of one-year, this equates to the  
 590 transformation  $\approx 5$  – 15 kg of Hg(II) to Hg(0). Even a relatively conservative estimate of the  
 591 conversion (and potential loss) of this mass of Hg(II) in contaminated aquifers such as this provides  
 592 strong evidence that the process of Hg(II) reduction plays a key role in limiting the transport of the  
 593 10-20 tonnes of Hg that was added to this soil-groundwater system in the  $\approx 120$  years since industrial  
 594 operations commenced.

### 595 3.3 Retardation ( $R_D$ ) and sorption coefficient ( $K_D$ ) calculations

596 As expected,  $R_D$  values were substantially greater than 1, confirming substantial interaction  
 597 between the applied HgCl<sub>2</sub> solution and the solid-phase aquifer materials (Table 3). The difference  
 598 in  $R_D$  and  $K_D$  values between EXP1 and EXP2 (Table 3) indicate stock solution concentration is a factor  
 599 in the transport of mercury within these columns. The elevated stock solution concentrations may  
 600 be undermining the assumption of equal accessibility to sorption sites (USEPA, 2004). However, the  
 601 purpose of these experiments was to simulate the original contamination by the industrial (mis)use  
 602 of HgCl<sub>2</sub> solution, and while we can only estimate original concentration of solution being  
 603 transported through the soil-groundwater system, we do expect they were very high due to the  
 604 extent (both in terms of elevated concentrations and longitudinal and transverse dispersion of the  
 605 contamination plume) of contamination that remains and the very high concentration of the  
 606 solution used in rot-prevention treatment of timber (Bollen et al., 2008; Richard et al., 2016a;  
 607 McLagan et al., 2022). Considering the high concentrations of Hg that have been observed within  
 608 this and other Hg contaminated aquifers (Katsenovich et al., 2010; Lamborg et al., 2013; Demers et  
 609 al., 2018), it is critical that we do not isolate our study of Hg transport dynamics to low concentration  
 610 experiments that meet assumptions for theoretical sorption (batch and column) experiments.

611 *Table 3: Calculated retardation ( $R_D$ ) and sorption ( $K_D$ ) coefficients for EXP1 and EXP2 (definitions are*  
 612 *given in Section 2.2.5).*

EXP1					EXP2				
Column	$t_w$ (min)	$t_{Hg}$ (min)	$R_D$	$K_D$ (mL g <sup>-1</sup> )	Column	$t_w$ (min)	$t_{Hg}$ (min)	$R_D$	$K_D$ (mL g <sup>-1</sup> )
C1.1	48.9	3628	74.7	23.8	C2.1	43.0	1615	37.6	11.8
C1.2	41.0	3629	88.5	29.5	C2.2	38.2	1567	41.2	12.9
C1.3	50.0	3779	75.6	25.1	C2.3	45.8	1837	39.9	12.6
C1.4	49.5	3678	74.3	-	C2.6	41.0	1438	35.1	-
C1.5	44.0	3488	79.3	-	C2.7	44.1	1623	36.9	-
C1.6	47.8	3599	75.3	-	C2.8	37.5	1317	35.1	-
		<b>Mean</b>	<b>77.9</b>	<b>26.1</b>			<b>Mean</b>	<b>38.4</b>	<b>12.4</b>
		<b>SD</b>	<b>5.5</b>	<b>3.0</b>			<b>SD</b>	<b>2.7</b>	<b>0.6</b>

613

614  $R_D$  values can be calculated from Miretzky et al. (2005) based on the inverse of their  $v/v_{\text{water}}$  value  
615 and the mean of these derived  $R_D$  values is  $48 \pm 13$  for the high OM Amazonian soils. This again  
616 affirms the high sorptive capacity of our low OM solid-phase aquifer materials at these comparative  
617 concentration  $\text{HgCl}_2$  applications. Lamborg et al. (2013) calculated  $K_D$  values for a Hg contaminated  
618 (from wastewater treatment) aquifer between 100 and 6300  $\text{mL g}^{-1}$  ( $\log K_D$ : 2-3.8); yet calculations  
619 had to assume liquid-phase concentrations from other studies.  $\log K_D$  values calculated from soil  
620 and sediment batch experiments typically range from  $\approx 2$  in lower OM materials (Akçay et al., 1996)  
621 up to  $\approx 6$  in higher OM materials (Lyon et al., 1997). The logical next step is to utilise the measured  
622  $R_D$  and  $K_D$  data from our study to perform soil-groundwater modelling to better understand Hg  
623 transport in this and other soil-groundwater systems as there are no previous estimates of  $R_D$  and  
624  $K_D$  values based on measured data for low OM solid-phase aquifer materials. The range of coefficient  
625 values from ours and other studies described above relating to differing solid-phase properties,  
626 input solution speciation, and assumptions used highlights the caution that should be made applying  
627 these values to other systems as  $R_D$  and  $K_D$  values tend to be highly site specific (USEPA, 2004).

## 628 Acknowledgements

629 We would like to thank Adelina Caean and Petra Schmidt for their support and contributions in  
630 terms of experimental setup and sample analyses (including A.C. travelling to Vienna for to assist  
631 with isotope analyses). We also thank undergraduate students Jan Pietrucha, Jette Greiser, and  
632 Katja Braun for helping with liquid-phase sample collection and analyses. We thank Stephan M.  
633 Kraemer for supporting the Hg isotope analyses at the University of Vienna. We would also like to  
634 acknowledge Thomas Schöndorf from HPC Environmental Consulting for providing the solid-phase  
635 materials used in this study. Also thanks to Hans Esser for helping design the eight-column holding  
636 rack used in the experiments. This research was funded by the German Science Foundation (DFG)  
637 grant BI 734/17-1 to H.B. and the Austrian Science Fund (FWF) grant I-3489-N28 to J.W. D.S.M.  
638 would like to thank for support provided through a National Sciences and Engineering Research  
639 Council of Canada (NSERC) postdoctoral fellowship.

## 640 Author contributions

641 D.S.M., C.E., and H.B. designed the study and experiments with some feedback from other co-  
642 authors, particularly J.-H.R during preliminary experiments. C.E. led all concentration and speciation  
643 analyses with assistance from D.S.M. Isotope analyses were led by L.S. with assistance from J.W.  
644 (and A.C. see above). This work was the basis for C.E.'s master's thesis, which was written in German.  
645 The manuscript first draft was written by D.S.M. and all other authors provided feedback in building  
646 the manuscript towards submission. Figures, tables, and SI were produced by D.S.M, C.E., and L.S.

## 647 References

- 648 Andersson, A.: Mercury in soil, In: The biochemistry of mercury in the environment, edited by:  
649 Nriagu, J. O., Elsevier, Amsterdam, Holland, 79-112, ISBN: 0444801103, 1979.
- 650 Akçay, H., Kiliç, S. İ. B. E. L., and Karapire, C.: A comparative study on the sorption and desorption  
651 of Hg, Th and U on clay, J. Radioanal. Nucl. Chem., 214, 51-66, <https://doi.org/10.1007/bf02165058>,  
652 1996.
- 653 Avotins, P. V.: Adsorption and coprecipitation studies of mercury on hydrous iron oxide, Stanford  
654 University, Stanford, USA, ISBN: 9798660526602, 1975.

655 Bergquist, B. A., and Blum, J. D.: Mass-dependent and-independent fractionation of Hg isotopes by  
656 photoreduction in aquatic systems, *Science*, 318, 417-420,  
657 <https://doi.org/10.1126/science.1148050>, 2007.

658 Bergquist, B. A., and Blum, J. D.: The odds and evens of mercury isotopes: applications of mass-  
659 dependent and mass-independent isotope fractionation, *Elements*, 5, 353-357,  
660 <https://doi.org/10.2113/gselements.5.6.353>, 2009.

661 Bloom, N. S., Preus, E., Katon, J., and Hiltner, M.: Selective extractions to assess the  
662 biogeochemically relevant fractionation of inorganic mercury in sediments and soils, *Anal. Chim.*  
663 *Acta*, 479, 233-248, [https://doi.org/10.1016/S0003-2670\(02\)01550-7](https://doi.org/10.1016/S0003-2670(02)01550-7), 2003.

664 Bollen, A., Wenke, A., and Biester, H.: Mercury speciation analyses in HgCl<sub>2</sub>-contaminated soils and  
665 groundwater—implications for risk assessment and remediation strategies, *Water Res.*, 42, 91-100,  
666 <https://doi.org/10.1016/j.watres.2007.07.011>, 2008.

667 Brocza, F. M., Biester, H., Richard, J. H., Kraemer, S. M., and Wiederhold, J. G.: Mercury isotope  
668 fractionation in the subsurface of a Hg(II) chloride-contaminated industrial legacy site, *Environ. Sci.*  
669 *Technol.*, 53, 7296-7305, <https://doi.org/10.1021/acs.est.9b00619>, 2019.

670 Bradl, H. B.: Adsorption of heavy metal ions on soils and soils constituents, *J. Colloid Interf. Sci.*, 277,  
671 1-18, <https://doi.org/10.1016/j.jcis.2004.04.005>, 2004.

672 Clarkson, T. W.: The toxicology of mercury, *Crit. Rev. Clinic. Lab. Sci.*, 34, 369-403,  
673 <https://doi.org/10.3109/10408369708998098>, 1997.

674 Demers, J. D., Blum, J. D., Brooks, S. C., Donovan, P. M., Riscassi, A. L., Miller, C. L., Zheng, W. and  
675 Gu, B.: Hg isotopes reveal in-stream processing and legacy inputs in East Fork Poplar Creek, Oak  
676 Ridge, Tennessee, USA, *Environ. Sci. Process. Impacts*, 20, 686-707,  
677 <https://doi.org/10.1039/C7EM00538E>, 2018.

678 DIN ISO: Method 11277: Soil quality—Determination of particle size distribution in mineral soil  
679 material—Method by sieving and sedimentation, German Institute for Standardisation (Deutsches  
680 Institut für Normung; DIN) International Organization for Standardization (ISO), Berlin, Germany,  
681 2002.

682 DIN: Method 1483: Water quality - Determination of mercury - Method using atomic absorption  
683 spectrometry, German Institute for Standardisation (Deutsches Institut für Normung; DIN), Berlin,  
684 Germany, 2007.

685 DIN: 19528-01: Leaching of solid materials - Percolation method for the joint examination of the  
686 leaching behaviour of organic and inorganic substances for materials with a particle size up to 32  
687 mm - Basic characterization using a comprehensive column test and compliance test using a quick  
688 column test, German Institute for Standardisation (Deutsches Institut für Normung; DIN), Berlin,  
689 Germany, 2009.

690 Gabriel, M. C., and Williamson, D. G.: Principal biogeochemical factors affecting the speciation and  
691 transport of mercury through the terrestrial environment, *Environ. Geochem. Health*, 26, 421-434,  
692 <https://doi.org/10.1007/s10653-004-1308-0>, 2004.

693 Gettens, R. J., Feller, R. L., and Chase, W. T.: Vermilion and cinnabar. *Stud. Conserv.*, 17, 45-69,  
694 <https://doi.org/10.1179/sic.1972.006>, 1972.

695 Goix, S., Maurice, L., Laffont, L., Rinaldo, R., Lagane, C., Chmeleff, J., Menges, J., Heimbürger, L.E.,  
696 Maury-Brachet, R. and Sonke, J. E.: Quantifying the impacts of artisanal gold mining on a tropical  
697 river system using mercury isotopes, *Chemosphere*, 219, 684-694,  
698 <https://doi.org/10.1016/j.chemosphere.2018.12.036>, 2019.

699 Grigg, A. R., Kretzschmar, R., Gilli, R. S., and Wiederhold, J. G.: Mercury isotope signatures of digests  
700 and sequential extracts from industrially contaminated soils and sediments, *Sci. Tot. Environ.*, 636,  
701 1344-1354, <https://doi.org/10.1016/j.scitotenv.2018.04.261>, 2018.

702 Gu, B., Bian, Y., Miller, C. L., Dong, W., Jiang, X., and Liang, L.: Mercury reduction and complexation  
703 by natural organic matter in anoxic environments, *Proceed. Nat. Acad. Sci.*, 108, 1479-1483,  
704 <https://doi.org/10.1073/pnas.1008747108>, 2011.

705 Gunneriusson, L. and Sjöberg, S.: Surface complexation in the H<sup>+</sup>-goethite ( $\alpha$ -FeOOH)-Hg (II)-  
706 chloride system, *J. Colloid Interf. Sci.* 156, 121-128, <https://doi.org/10.1006/jcis.1993.1090>, 1993.

707 Haitzer, M., Aiken, G. R., and Ryan, J. N.: Binding of mercury (II) to dissolved organic matter: the role  
708 of the mercury-to-DOM concentration ratio, *Environ. Sci. Technol.*, 36, 3564-3570,  
709 <https://doi.org/10.1021/es025699i>, 2002.

710 Hall, G. E., Pelchat, J. C., Pelchat, P., and Vaive, J. E.: Sample collection, filtration and preservation  
711 protocols for the determination of 'total dissolved' mercury in waters, *Analyst*, 127, 674-680,  
712 <https://doi.org/10.1039/B110491H>, 2002.

713 Hammerschmidt, C. R., Bowman, K. L., Tabatchnick, M. D., and Lamborg, C. H.: Storage bottle  
714 material and cleaning for determination of total mercury in seawater, *Limnol. Oceanogr.*  
715 *Methods*, 9, 426-431, <https://doi.org/10.4319/lom.2011.9.426>, 2011.

716 Hebig, K. H., Nödler, K., Licha, T., and Scheytt, T. J.: Impact of materials used in lab and field  
717 experiments on the recovery of organic micropollutants, *Sci. Tot. Environ.*, 473, 125-131,  
718 <https://doi.org/10.1016/j.scitotenv.2013.12.004>, 2014.

719 Ho, T. L.: Hard soft acids bases (HSAB) principle and organic chemistry, *Chem. Rev.*, 75, 1-20,  
720 <https://doi.org/10.1021/cr60293a001>, 1975.

721 Jiskra, M., Wiederhold, J. G., Bourdon, B., and Kretzschmar, R.: Solution speciation controls mercury  
722 isotope fractionation of Hg(II) sorption to goethite. *Environ. Sci. Technol.*, 46, 6654-6662,  
723 <https://doi.org/10.1021/es3008112>, 2012.

724 Jiskra, M., Wiederhold, J. G., Skyllberg, U., Kronberg, R. M., and Kretzschmar, R.: Source tracing of  
725 natural organic matter bound mercury in boreal forest runoff with mercury stable isotopes, *Environ.*  
726 *Sci. Process. Impacts*, 19, 1235-1248, <https://doi.org/10.1039/C7EM00245A>, 2017.

727 Katsenovich, Y., Tachiev, G., Fuentes, H. R., Roelant, D., and Henao, A.: A study of the mercury (II)  
728 sorption and transport with Oak Ridge Reservation soil, *Waste Management Conference 2010*,  
729 Phoenix, USA, <https://archivedproceedings.econference.io/wmsym/2010/pdfs/10222.pdf>, 2010.

730 Kim, C. S., Rytuba, J. J., and Brown Jr, G. E.: EXAFS study of mercury (II) sorption to Fe-and Al-(hydr)  
731 oxides: II. Effects of chloride and sulfate, *J. Colloid Interf. Sci.*, 270, 9-20,  
732 <https://doi.org/10.1016/j.jcis.2003.07.029>, 2004.

- 733 Kocman, D., Horvat, M., Pirrone, N., and Cinnirella, S.: Contribution of contaminated sites to the  
734 global mercury budget, *Environ. Res.*, 125, 160-170, <https://doi.org/10.1016/j.envres.2012.12.011>,  
735 2013.
- 736 Lamborg, C. H., Kent, D. B., Swarr, G. J., Munson, K. M., Kading, T., O'Connor, A. E., Fairchild, G. M.,  
737 LeBlanc, D. R., and Wiatrowski, H. A.: Mercury speciation and mobilization in a wastewater-  
738 contaminated groundwater plume, *Environ. Sci. Technol.*, 47, 13239-13249,  
739 <https://doi.org/10.1021/es402441d>, 2013.
- 740 Leterme, B., Blanc, P., and Jacques, D.: A reactive transport model for mercury fate in soil—  
741 application to different anthropogenic pollution sources, *Environ. Sci. Poll. Res.*, 21, 12279-12293,  
742 <https://doi.org/10.1007/s11356-014-3135-x>, 2014.
- 743 Lewis, J., and Sjöström, J.: Optimizing the experimental design of soil columns in saturated and  
744 unsaturated transport experiments, *J. Contam. Hydrol.*, 115, 1-13,  
745 <https://doi.org/10.1016/j.jconhyd.2010.04.001>, 2010.
- 746 Lockwood, R. A., and Chen, K. Y.: Adsorption of mercury (II) by hydrous manganese oxides, *Environ.*  
747 *Sci. Technol.*, 7, 1028-1034, <https://doi.org/10.1021/es60083a006>, 1973.
- 748 Llanos, W., Kocman, D., Higuera, P., and Horvat, M.: Mercury emission and dispersion models from  
749 soils contaminated by cinnabar mining and metallurgy, *J. Environ. Monit.*, 13, 3460-3468,  
750 <https://doi.org/10.1039/C1EM10694E>, 2011.
- 751 Lu, Y. F., Wu, Q., Yan, J. W., Shi, J. Z., Liu, J., and Shi, J. S.: Realgar, cinnabar and An-Gong-Niu-Huang  
752 Wan are much less chronically nephrotoxic than common arsenicals and mercurial, *Exp. Biol.*  
753 *Med.*, 236, 233-239, <https://doi.org/10.1258/ebm.2010.010247>, 2011.
- 754 Lyon, B. F., Ambrose, R., Rice, G., and Maxwell, C. J.: Calculation of soil-water and benthic sediment  
755 partition coefficients for mercury, *Chemosphere*, 35, 791-808, [https://doi.org/10.1016/S0045-](https://doi.org/10.1016/S0045-6535(97)00200-2)  
756 [6535\(97\)00200-2](https://doi.org/10.1016/S0045-6535(97)00200-2), 1997.
- 757 Manceau, A., and Nagy, K. L.: Thiols in natural organic matter: Molecular forms, acidity, and  
758 reactivity with mercury (II) from First-Principles calculations and high energy-resolution X-ray  
759 absorption near-edge structure spectroscopy, *ACS Earth Space Chem.*, 3, 2795-2807,  
760 <https://doi.org/10.1021/acsearthspacechem.9b00278>, 2019.
- 761 McLagan, D. S., Schwab, L., Wiederhold, J. G., Chen, L., Pietrucha, J., Kraemer, S. M., and Biester, H.:  
762 Demystifying mercury geochemistry in contaminated soil-groundwater systems with  
763 complementary mercury stable isotope, concentration, and speciation analyses, *Environ. Sci.*  
764 *Process. Impacts*, 24, 1406-1429, <https://doi.org/10.1039/D1EM00368B>, 2022.
- 765 Miretzky, P., Bisinoti, M. C., & Jardim, W. F.: Sorption of mercury (II) in Amazon soils from column  
766 studies, *Chemosphere*, 60, 1583-1589, <https://doi.org/10.1016/j.chemosphere.2005.02.050>, 2005.
- 767 Norrby, L. J.: Why is mercury liquid? Or, why do relativistic effects not get into chemistry  
768 textbooks? *J. Chem. Ed.*, 68, 110, <https://doi.org/10.1021/ed068p110>, 1991.
- 769 Obrist, D., Agnan, Y., Jiskra, M., Olson, C. L., Colegrove, D. P., Hueber, J., Moore, C.W., Sonke, J.E.  
770 and Helmig, D.: Tundra uptake of atmospheric elemental mercury drives Arctic mercury  
771 pollution, *Nature*, 547, 201-204, <https://doi.org/10.1038/nature22997>, 2017.

772 Parker, J. L., and Bloom, N. S.: Preservation and storage techniques for low-level aqueous mercury  
773 speciation, *Sci. Tot. Environ.*, 337, 253-263, <https://doi.org/10.1016/j.scitotenv.2004.07.006>, 2005.

774 Patterson, B. M., Pribac, F., Barber, C., Davis, G. B., and Gibbs, R.: Biodegradation and retardation of  
775 PCE and BTEX compounds in aquifer material from Western Australia using large-scale columns, *J.*  
776 *Contam. Hydrol.*, 14, 261-278, [https://doi.org/10.1016/0169-7722\(93\)90028-Q](https://doi.org/10.1016/0169-7722(93)90028-Q), 1993.

777 Pirrone, N., Cinnirella, S., Feng, X., Finkelman, R.B., Friedli, H.R., Leaner, J., Mason, R., Mukherjee,  
778 A.B., Stracher, G.B., Streets, D.G. and Telmer, K.: Global mercury emissions to the atmosphere from  
779 anthropogenic and natural sources, *Atmos. Chem. and Phys.*, 10, 5951-5964,  
780 <https://doi.org/10.5194/acp-10-5951-2010>, 2010.

781 Reis, A. T., Davidson, C. M., Vale, C., and Pereira, E.: Overview and challenges of mercury  
782 fractionation and speciation in soils, *Trends Anal. Chem.*, 82, 109-117,  
783 <https://doi.org/10.1016/j.trac.2016.05.008>, 2016.

784 Richard, J. H., Bischoff, C., and Biester, H.: Comparing modeled and measured mercury speciation in  
785 contaminated groundwater: Importance of dissolved organic matter composition, *Environ. Sci.*  
786 *Technol.*, 50, 7508-7516, <https://doi.org/10.1016/j.trac.2016.05.008>, 2016a.

787 Richard, J. H., Bischoff, C., Ahrens, C. G., and Biester, H.: Mercury (II) reduction and co-precipitation  
788 of metallic mercury on hydrous ferric oxide in contaminated groundwater, *Sci. Tot. Environ.*, 539,  
789 36-44, <https://doi.org/10.1016/j.scitotenv.2015.08.116>, 2016b.

790 Sentenac, P., Lynch, R. J., and Bolton, M. D.: Measurement of a side-wall boundary effect in soil  
791 columns using fibre-optics sensing, *Int. J. Phys. Model. Geotech.*, 1, 35-41,  
792 <https://doi.org/10.1680/ijpmg.2001.010404>, 2001.

793 Sanemasa, I.: The solubility of elemental mercury vapor in water, *Bull. Chem. Soc. Jpn.*, 48, 1795-  
794 1798, <https://doi.org/10.1246/bcsj.48.1795>, 1975

795 Schroeder, W. H., and Munthe, J.: Atmospheric mercury—an overview, *Atmos. Environ.*, 32, 809-  
796 822, [https://doi.org/10.1016/S1352-2310\(97\)00293-8](https://doi.org/10.1016/S1352-2310(97)00293-8), 1998.

797 Schlüter, K., Seip, H. M., and Alstad, J.: Mercury translocation in and evaporation from soil. II.  
798 Evaporation of mercury from podzolized soil profiles treated with HgCl<sub>2</sub> and CH<sub>3</sub>HgCl, *Soil Sediment*  
799 *Contam.*, 4, 269-298, <https://doi.org/10.1080/15320389509383498>, 1995.

800 Schlüter, K.: Sorption of inorganic mercury and monomethyl mercury in an iron–humus podzol soil  
801 of southern Norway studied by batch experiments, *Environ. Geol.*, 30, 266-279,  
802 <https://doi.org/10.1007/s002540050156>, 1997.

803 Schnaar, G., and Brusseau, M. L.: Measuring equilibrium sorption coefficients with the miscible-  
804 displacement method, *J Environ. Sci. Health A*, 48, 355-359,  
805 <https://doi.org/10.1080/10934529.2013.727733>, 2013.

806 Schöndorf, T., Egli, M., Biester, H., Mailahn, W., and Rotard, W.: Distribution, Bioavailability and  
807 Speciation of Mercury in Contaminated Soil and Groundwater of a Former Wood Impregnation  
808 Plant, in: *Mercury Contaminated Sites*, edited by: Ebinghaus, R., Turner, R.R., de Lacerda, L.D.,  
809 Vasiliev, O., Salomons, W., Springer, Berlin, Heidelberg, 181-206, [https://doi.org/10.1007/978-3-662-03754-6\\_9](https://doi.org/10.1007/978-3-662-03754-6_9), 1999.

811 Schuster, E.: The behavior of mercury in the soil with special emphasis on complexation and  
812 adsorption processes-a review of the literature, *Water Air Soil Poll.*, 56, 667-680,  
813 <https://doi.org/10.1007/BF00342308>, 1991.

814 Schuster, P. F., Shanley, J. B., Marvin-Dipasquale, M., Reddy, M. M., Aiken, G. R., Roth, D. A., Taylor,  
815 H. E., Krabbenhoft, D. P. and DeWild, J. F.: Mercury and organic carbon dynamics during runoff  
816 episodes from a northeastern USA watershed, *Water Air Soil Poll.*, 187, 89-108,  
817 <https://doi.org/10.1007/s11270-007-9500-3>, 2008.

818 Schwab, L., Gallati, N., Reiter, S.M., Kimber, R.L., Kumar, N., McLagan, D.S., Biester, H., Kraemer,  
819 S.M. and Wiederhold, J.G.: Mercury Isotope Fractionation during Dark Abiotic Reduction of Hg (II)  
820 by Dissolved, Surface-Bound, and Structural Fe (II), *Environ. Sci. Technol.*, 57, 15243-15254,  
821 <https://doi.org/10.1021/acs.est.3c03703>, 2023.

822 Skyllberg, U.: Chemical speciation of mercury in soil and sediment, in: *Environmental chemistry and*  
823 *toxicology of mercury*, edited by: Liu, G., Cai, Y., Driscoll, N., Wiley & Sons Inc., Hoboken, USA, 219-  
824 258, <https://doi.org/10.1002/9781118146644.ch7>, 2012.

825 Streets, D. G., Horowitz, H. M., Lu, Z., Levin, L., Thackray, C. P., and Sunderland, E. M.: Global and  
826 regional trends in mercury emissions and concentrations, 2010–2015, *Atmos. Environ.*, 201, 417-  
827 427, <https://doi.org/10.1016/j.atmosenv.2018.12.031>, 2019.

828 Ullrich, S. M., Tanton, T. W., and Abdrashitova, S. A.: Mercury in the aquatic environment: a review  
829 of factors affecting methylation, *Crit. Rev. Environ. Sci. Technol.*, 31, 241-293,  
830 <https://doi.org/10.1080/20016491089226>, 2001.

831 USEPA.: Method 1631, Revision E: Mercury in water by oxidation, purge and trap, and cold vapor  
832 atomic fluorescence spectrometry, United States Environmental Protection Agency (USEPA),  
833 Washington, DC, 2002.

834 USEPA.: Understanding variation in partition coefficient, K<sub>d</sub>, values. Volume III: Review of  
835 Geochemistry and Available K<sub>d</sub> Values for Americium, Arsenic, Curium, Iodine, Neptunium, Radium,  
836 and Technetium. United States Environmental Protection Agency (USEPA), Washington, DC, USA,  
837 2004.

838 Van Genuchten, M. T., and Parker, J. C.: Boundary conditions for displacement experiments through  
839 short laboratory soil columns, *Soil Sci. Soc. Am. J.*, 48, 703-708,  
840 <https://doi.org/10.2136/sssaj1984.03615995004800040002x>, 1984.

841 Van Glubt, S., Brusseau, M. L., Yan, N., Huang, D., Khan, N., and Carroll, K. C.: Column versus batch  
842 methods for measuring PFOS and PFOA sorption to geomeia. *Environ. Poll.*, 268, 115917,  
843 <https://doi.org/10.1016/j.envpol.2020.115917>, 2021

844 Wiederhold, J. G., Cramer, C. J., Daniel, K., Infante, I., Bourdon, B., and Kretzschmar, R.: Equilibrium  
845 mercury isotope fractionation between dissolved Hg (II) species and thiol-bound Hg, *Environ. Sci.*  
846 *Technol.*, 44, 4191-4197, <https://doi.org/10.1021/es100205t>, 2010.

847 Wiederhold, J. G.: Metal stable isotope signatures as tracers in environmental geochemistry,  
848 *Environ. Sci. Technol.*, 49, 2606-2624, <https://doi.org/10.1021/es504683e>, 2015.

849 Yin, Y., Allen, H. E., Li, Y., Huang, C. P., and Sanders, P. F.: Adsorption of mercury (II) by soil: effects  
850 of pH, chloride, and organic matter, *J. Environ. Qual.*, 25, 837-844,  
851 <https://doi.org/10.2134/jeq1996.00472425002500040027x>, 1996.

- 852 Yin, Y., Allen, H. E., Huang, C., Sparks, D. L., and Sanders, P. F.: Kinetics of mercury (II) adsorption and  
853 desorption on soil, *Environ. Sci. Technol.*, 31, 496-503, <https://doi.org/10.1021/es9603214>, 1997.
- 854 Zheng, W., and Hintelmann, H.: Nuclear field shift effect in isotope fractionation of mercury during  
855 abiotic reduction in the absence of light, *J. Phys. Chem. A*, 114, 4238-4245,  
856 <https://doi.org/10.1021/jp910353y>, 2010.